2008

Magnetic study of magnetite (Fe_3O_4) nanoparticles

Maninder Kaur Tarsem Singh
San Jose State University

MAGNETIC STUDY OF MAGNETITE (Fe_3O_4) NANOPARTICLES

A Thesis

Presented to

The Faculty of the Department of Physics

San Jose State University

In Partial Fulfillment

of the Requirements for the Degree

Master of Science

by

Maninder Kaur Tarsem Singh

August 2008

APPROVED FOR THE DEPARTMENT OF PHYSICS

Dr. Kiumars Parvin

Dr. Carel Boekema

Dr. Ramen Bahuguna

APPROVED FOR THE UNIVERSITY

Rhea I. Williamson 07/18/08

ABSTRACT
MAGNETIC STUDY OF MAGNETITE (Fe_3O_4) NANOPARTICLES

by Maninder Kaur Tarsem Singh

Magnetite Fe_3O_4 nanoparticles with the size in the range $3-5$ nm have been synthesized using self-assembly method of Sun and Zeng. X-ray diffraction profile of nanoparticles shows all major peaks associated with crystalline Fe_3O_4, and yields the average particle size of 3.56 nm from width of the peaks. Dark field transmission electron microscope images indicate that the particles have a tight size distribution and are almost spherical. Electron dispersive spectroscopy spectrum identifies the elements iron and oxygen in the nanoparticles with their atomic percentages consistent with Fe_3O_4. Magnetization measurements have been carried out utilizing a vibrating sample magnetometer over the temperature range $4.2-300$ K. Zero-field-cooled and field-cooled magnetization versus temperature gives a blocking temperature of $T_B = 20$ K. The M-H curves above T_B fit well to the Langevin function and reveal the super-paramagnetism nature of nanoparticles. M-H curves below T_B indicate the ferromagnetic behavior with coercive field H_c = 37-190 Oe for temperature range 6.5-18.5 K.

ACKNOWLEDGEMENTS

I owe my deepest gratitude to my advisor Professor Kiumars Parvin. His guidance has carried forward this project at every crucial step, I have also benefited tremendously through his pedagogy in the classroom. I can only aspire to inherit a portion of his wisdom and clarity in thinking. Thank you also for the patience and the space to evolve. I am also very thankful for the help and encouragement I received from all the professors in the Physics Department; especially to Prof. Boekema and Prof. Bahuguna for reviewing my thesis and serving on the committee.

I would also like to thank the SJSU Physics Department staff Bertha Aguayo and technical staff Pat Joyce, Minh Mai, and Jose Garcia. I am thankful to all my friends and the WiSE people.

Finally, I thank my parents and brothers for their unaltering confidence in my abilities and their invaluable support.

TABLE OF CONTENTS

FIGURES

CHAPTER 1

INTRODUCTION

Magnetic nanoparticles have generated considerable interest since 1940s when investigation of their properties turned out to be exciting from scientific and technological point of view. Neel (1949) observed that the characteristic magnetic properties of particles are quite different from bulk materials. He found that iron in grains smaller than 32 nm are single domain and have a high coercive field at room temperature. Jacob and Bean (1963) measured the magnetization of 4.4-nm iron particles. They measured magnetization versus field curves with zero coercive field at 200 K and 77 K and non-zero coercive field at 5 K indicating the significant role of temperature in the properties of nanoparticles. Kneller and Luborsky (1963) studied the dependence of coercive field and remanence on particle size in 40% atomic iron and 60% atomic cobalt particles. The plot of coercive field versus particle size at temperature 4 K showed a maximum coercive field for single domain particles of diameter D_s equal to 26.1 nm and smaller coercive field for particles with diameter $D > D_s$ and zero coercive field for $D \ll D_s$. The above three size characteristic regions are referred to as single domain $(D = D_s)$, multidomain $(D > D_s)$, and superparamagnet $(D \ll D_s)$. This

investigation indicates that the size of particles can be adjusted to obtain the required magnetic property at specific temperature.

In 1985 the carbon arc method was developed for synthesis of carbon-coated nanoparticles (Ruoff, Lorents, Chan, Malhotra, and Subramoney, 1993). In this method the powder of metal or metal oxide were placed in a hole drilled in the anode of an arc chamber made of graphite. The generation of arc produced carbon-coated nanoparticles that were collected from the walls of the chamber. In the graphite-encapsulated nanoparticles the carbon layer prevents the oxidation of nanoparticles. Moreover, the graphite coating decreases the magnetic interaction of neighboring particles by increasing their distance, which is an important issue from application point of view.

Several groups have reported the synthesis and characterization of magnetic carbon-coated nanoparticles in the past two decades. To mention a few, Subramoney, Ruoff, Lorents, Chan, Malhotra, Dayer, and Parvin (1994) studied the encapsulated gadolinium nanoparticles; Mchenry, Majetich, Artman, DeGraef, and Staley (1994) synthesized cobalt nanoparticles encapsulated in carbon polyhedra; and Hihara, Onodera, Sumiyama, Suzuki, Kasuya, Nishina, et al. (1994) studied graphite coated iron nanoparticles. The major problem with this method was the production of large amount of undesirable carboneous materials that made the magnetic measurements difficult to analyze. This method was replaced by tungsten arc method developed by Dravid, Host, Teng, Elliot, Hwang, Johnson, et al. (1995) in which very small amount of carbonaceous material was produced during synthesis. Gong, Li, Zhao, and Chen (1993) and Gangopadhyay,

Hadjipanayis, Dale, Sorensen, and K. J. (1992) studied the magnetic properties of unencapsulated cobalt nanoparticles and observed that high coercive field was associated with cobalt oxide layer that was coating the cobalt nanoparticles.

Sun and Murray (1999) synthesized cobalt nanoparticles with average size 8-10 nm using a chemical self-assembly method. In this method cobalt chloride is heated with oleic acid, dioctyl ether, and trialkylphosphine to temperature of 200^0 C. The injection of superhydride at this temperature reduced cobalt ions into cobalt nanoparticles. Later they demonstrated that with this synthesis method one may produce nanoparticles with a narrow size distribution (Woods, Kirtley, Sun, and Koch, 2001). Similar method was also used for synthesis of 4-nm face-centered cubic (fcc) iron platinum (FePt) nanoparticles (Sun, Murray, Weller, Folks, and A. M., 2000, Sun, Anders, Thomson, Baglin, Toney, Hamann, et al. 2003). This method consists of thermal decomposition of iron pentacarbonyl $Fe(CO)_5$ and reduction of platinum acetylacetonate $Pt(acac)_2$ at 200^0 C. The solution was also refluxed at 300^0 C, which resulted in the formation of fcc FePt nanoparticles. They also showed that heating at temperature 560^0 C causes the transformation of fcc FePt nanoparticles to face-centered tetragonal (fct) structure. In contrast to cobalt nanoparticles that transform from ferromagnet to superparamagnet below 8 nm at room temperature, fct iron platinum with a high magnetocrystalline anisotropy stays ferromagnet down to 4 nm.

Several other groups studied the synthesis and characterization of magnetic nanoparticles using the same self-assembly method. Elkins, Li, Poudyal, Nandwana, Jin,

Chen, and Liu (2005) reported monodisperse face centered tetragonal FePt nanoparticles with giant coercivity. In order to transform fcc to fct, they annealed the mixture of as prepared FePt particles mixed with salt powder. They observed that the particles did not agglomerate in the annealing process and a high coercive field of 30 kOe at room temperature for fct particles was measured. Kang, Harrell, and Nikles (2002) studied FePt nanoparticles with added silver. They found that the addition of silver results in transformation of fcc-FePt to fct-FePt nanoparticles at lower temperature.

Sun and Zeng (2002) reported the synthesis of monodisperse magnetite Fe_3O_4 nanoparticles of size 4 nm. The synthesis method consists of reaction of iron acetylacetonate with phenyl ether, alcohol, oleic acid, and oleylamine at 265^0 C. Their magnetic measurements indicated that these particles are superparamagnetic at room temperature.

In this work Fe_3O_4 nanoparticles were synthesized using the same method and magnetic properties were studied in more detail. Nanoparticles were synthesized at the University of Alabama MINT center by Dr. X.C. Sun. He also performed x-ray diffraction and transmission electron microscopy. We at San Jose State also performed x-ray diffraction and studied magnetic properties.

In Chapter 2 we present an introduction to magnetic materials, and in Chapter 3 we discuss the classical theory of paramagnetism. Chapter 4 is a discussion of the concept of superparamagnetism, which is the application of classical theory of paramagnetism to nanoparticles. Synthesis, experimental systems, and actual experiments performed on

Fe_3O_4 particles are discussed in Chapters 5, 6, and 7 respectively. We discuss results and analysis in Chapter 8.

CHAPTER 2

INTRODUCTION TO MAGNETIC MATERIALS

Magnetic materials are identified by their strength of magnetic dipole moments, which are due to electrons of the atom. An electron has orbital and spin magnetic dipole moment associated with orbital electron motion around the nucleus and spin of the electron respectively. Magnetization M of a material is the total dipole magnetic moment per unit volume or mass. The strength of magnetization depends on external magnetic field H.

Susceptibility χ is a physical quantity indicating how responsive a material is to an applied magnetic field H. It is defined as

$$\chi = \frac{dM}{dH} \tag{2.1}$$

Below we describe three major types of magnetic materials based on dependence of M on H or dependence of χ on H.

2.1 DIAMAGNETISM

The dependence of M on H is linear with small negative magnetic susceptibility resulting in the opposite directions of magnetization and applied field (Figure 1).

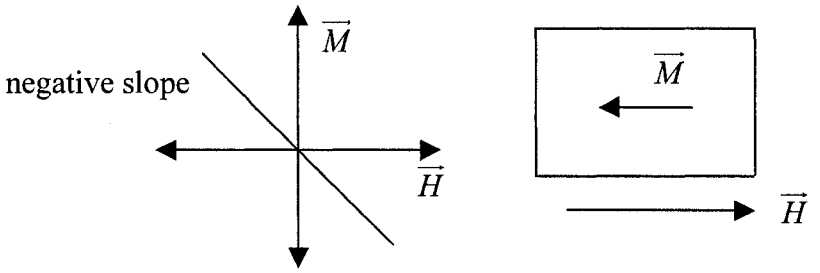

Figure 1. A diamagnetic material.

2.2 PARAMAGNETISM

The dependence of M on H is linear with small positive magnetic susceptibility resulting in the same direction for M and H (Figure 2). We will discuss this issue in more detail later.

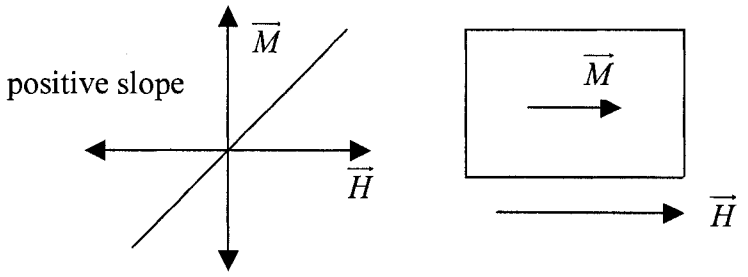

Figure 2. A paramagnetic material.

2.3 FERROMAGNETISM

The dependence of M on H is nonlinear with large positive magnetic susceptibility. The characteristic M versus H curve is known as hysteresis curve as shown in Figure 3.

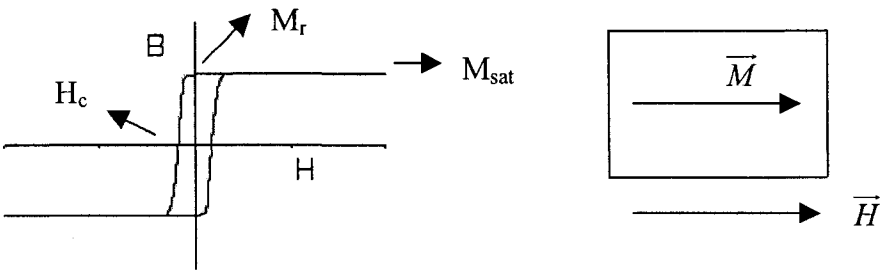

Figure 3. M vs H hysteresis curve.

M_{sat} is the saturation magnetization where all moments align along the direction of applied field. M_r is the remnant magnetization, which is remained in the material after applied field is removed. H_c is coercive field which is the field required to bring the magnetization to zero or demagnetize the sample.

2.4 FINE PARTICLES

A ferromagnetic material consists of small regions called domains inside which the magnetization has a single magnitude and direction (Figure 4).

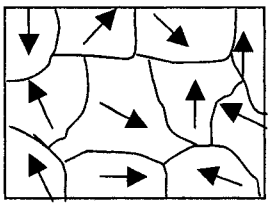

Figure 4. A ferromagnetic material.

When the material formed into a powder with the particle size equal to or smaller than the domain size, the material is referred to as single domain fine particle.

CHAPTER 3

CLASSICAL THEORY OF PARAMAGNETISM

Usually a paramagnetic material consists of non-interacting atoms (molecules) each with the net atomic (molecular) magnetic moment μ. In the absence of external applied field, the magnetic moments orient randomly to give zero net magnetic moment. In the presence of applied field, the magnitude of the total moment depends on the temperature T and applied field H. At low temperature, more dipole moments align in the direction of applied field, which result in the large net magnetic moment. On the other hand at high temperature magnetic moments are randomly oriented due to temperature effect and give small magnetic moment. Such an atomic (molecular) system is analyzed by quantum mechanics (Cullity, 1972).

Classical theory of paramagnetism can be applied to single domain particles where the carriers of magnetic moments are individual particles; and they have zero interaction with each other. Below we describe such classical theory for completeness although this theory is described in magnetic material texts (Spaldin, 2003).

3.1 LANGEVIN FUNCTION

Consider a unit volume of material containing n particles, each with moment $\vec{\mu}$. All μ vectors are drawn through the center of sphere of radius r. The number of moments dn aligned between azimuthal angle θ and $\theta+d\theta$ can be calculated as follow.

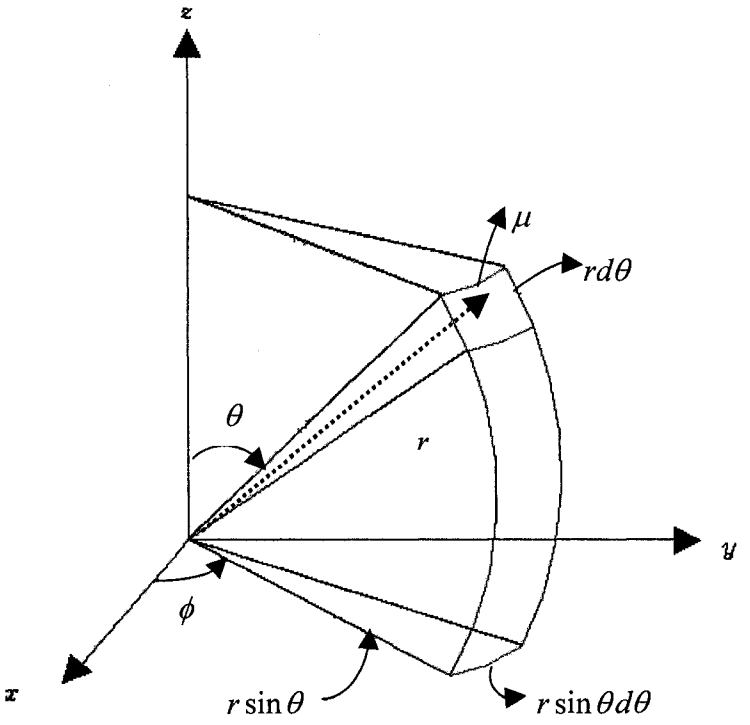

Figure 5. Effect of a field on orbital moments.

In the absence of external field due to randomized direction of moments the number of moments dn passing through area dA is proportional to $dA = 2\pi \sin\theta \, d\theta$.

$$dn = K(2\pi \sin\theta \, d\theta) \tag{3.1}$$

In presence of external field H, μ vectors direct along the direction of H. Each atomic moment has a potential energy E_p given by

$$E_p = -\mu H \cos\theta \tag{3.2}$$

The probability of a particle having energy E_p at temperature T is proportional to Boltzman factor $e^{-E_p/kT}$ where k is Boltzmann constant.

$$dn = K(2\pi \sin\theta \, d\theta) \, e^{\mu H\cos\theta/kT} \tag{3.3}$$

Integrating dn gives

$$n = \int dn = \int 2\pi K \, e^{\mu H\cos\theta/kT} \sin\theta \, d\theta = 2\pi K \int_0^{\pi} e^{a\cos\theta} \sin\theta \, d\theta \tag{3.4}$$

where

$$a = \frac{\mu H}{kT} \tag{3.5}$$

The component of magnetic moment μ along H (also z axis) is $\mu\cos\theta$. Total magnetization M along H is equal to product of number of moments and component of each moment along z-axis (Spaldin, 2003).

$$M = \int_0^n \mu\cos\theta \, dn = \frac{\mu n \int_0^{\pi} e^{a\cos\theta} \sin\theta\cos\theta d\theta}{\int_0^{\pi} e^{a\cos\theta} \sin\theta d\theta} = \mu n \left(\coth a - \frac{1}{a} \right) \tag{3.6}$$

Where μn is the maximum possible magnetic moment of sample of n particles each with magnetic moment μ along the direction of external field.

The function L(a) given by

$$L(a) = \frac{M}{\mu n} = \coth a - \frac{1}{a} \tag{3.7}$$

is called Langevin function.

Let $M_0 = \mu n$ and $a = \frac{\mu H}{k_B T}$

$$M = M_0 \left(\coth\left(\frac{\mu H}{k_B T} \right) - \frac{k_B T}{\mu H} \right) \tag{3.8}$$

L(a) versus $\frac{\mu H}{k_B T}$ is plotted in Figure 6.

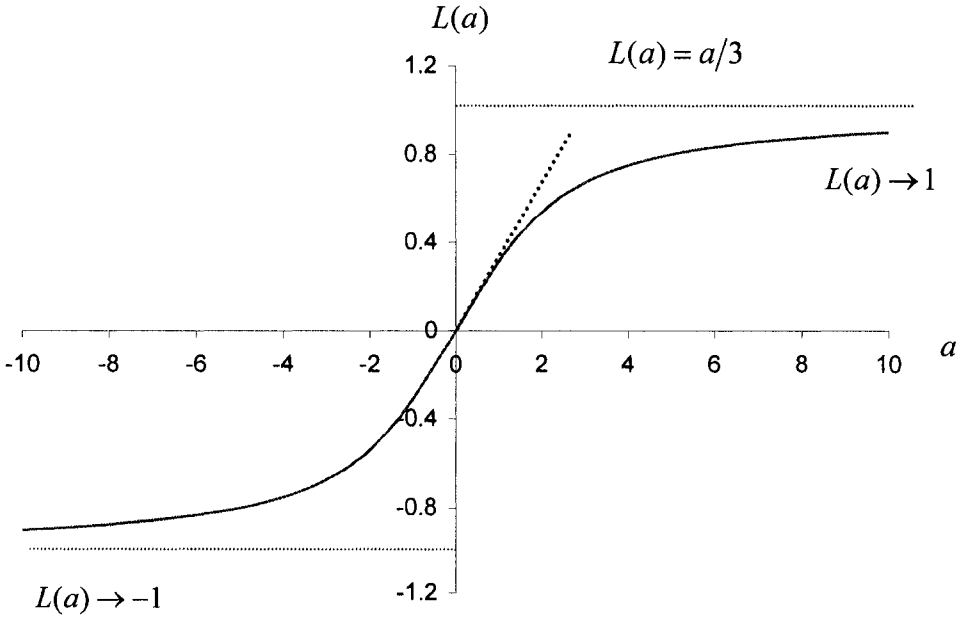

Figure 6. Langevin function.

At low temperature and high magnetic field, $a \gg 1$ $(L(a) \to 1)$ and the limiting expression for M becomes

$$M = M_0$$

which indicates complete alignment of all moments along the external field.

On the other hand at high temperature and low magnetic field $a \ll 1$ $(L(a) \to \frac{a}{3})$ and the limiting expression for M becomes

$$M = \frac{M_0 \mu H}{3k_B T} = \frac{n\mu^2 H}{3k_B T}, \tag{3.9}$$

the thermal effect randomizes the magnetic moments which is shown in Figure 6.
We used the fact that M is proportional to H to write $M = \chi H$ and obtained the expression for magnetic susceptibility χ as $\chi = \frac{C}{T}$ which is usually referred to as Curie law.

Quantum theory of paramagnetism is based on the fact that magnetic moments under consideration do not lie along any direction but are restricted to certain quantized directions. This situation does not apply to particles since particle magnetic moment direction is continuous and no quantization is required. Therefore we do not discuss this quantum theory here.

CHAPTER 4

FINE PARTICLES SUPERPARAMAGNETISM

4.1 MAGNETOCRYSTALLINE ANISOTROPY

Bulk materials exist may be in polycrystalline, amorphous or in single crystal form depending on their method of formation. Many materials are polycrystalline, that is, they are composed of many small crystals or grains oriented in different directions. This disorientation of grains gives no preferred direction to the material. Therefore magnetic properties of bulk material are independent of the direction of an applied magnetic field. A single crystal has its own specific crystalline axes. These axes show different magnetic response in the presence of an applied magnetic field. The dependence of magnetic property on a particular direction is known as magnetocrystalline anisotropy. The axis along which magnetization reaches saturation at lowest field is called easy axis. The term hard axis is used for the axis along which the largest field causes saturation magnetization.

Magnetocrystalline energy is the amount of energy required to turn the direction of magnetic moment away from an easy direction. For cubic crystal structure, it is given by

$$E_a = K_1\left(\cos^2\theta_1\cos^2\theta_2 + \cos^2\theta_2\cos^2\theta_3 + \cos^2\theta_3\cos^2\theta_1\right)$$

where $\theta_1,\theta_2,\theta_3$ are angles, which the magnetization makes relative to the three crystal axes.

4.2 SUPERPARAMAGNETISM

Consider an assembly of fine particles, each with an anisotropy energy density E given by $E = K\sin^2\theta$, where K is the uniaxial anisotropy constant and θ is the angle between saturation magnetization M_s and the easy axis. In order to reverse the magnetization, a particle must overcome the energy barrier $\Delta E = KV$ where V is the particle volume. When the size of a single domain particle is small enough, spontaneous reversal of magnetization occurs due to the thermal energy k_BT even in the absence of an applied field.

In a typical paramagnet the applied field will help moments to align in the direction of field, and thermal energy will tend to misalign them. This is the characteristic behavior of a normal paramagnetic material in which the magnetic moment under consideration is due to an ion or an atom and is usually a few Bohr magnetons. If a single domain particle is small enough such that the energy barrier KV is comparable to thermal energy k_BT, then this particle behaves like a paramagnet except it has a large moment. As an example a 10 A^0 spherical particle of iron contains 45 atoms, which gives the moment of $100\,\mu_B$ (moment of $2.2\,\mu_B$ per atom). Compared to an atom, the magnetic moment of such a fine particle is huge. Although the behavior of this particle system is

similar to a paramagnetic material, it is called superparamagnet due to its large individual particle moment.

Consider an assembly of non-interacting particles each with magnetic moment μ without any directional preference. The magnetization in the presence of an applied field H is explained by the classical theory of paramagnetism since there is no quantization requirement on individual particle moment. Using the classical statistical physics calculation one can show that the magnetization M of this assembly of particles at temperature T with magnetic field H is give by $M = M_0 L(a)$, where $M_0 = n\mu$ is the saturation magnetization, μ is the magnetic moment of each particle, n is the number of particles per unit volume, and L(a) is the Langevin function of $a = \mu H / k_B T$.

It is important to point out that magnetization curves at different temperatures superimpose when M/M_0 is plotted as a function of $\mu H / k_B T$. Also if we sweep the field back and forth the same curve of M vs. H is obtained indicating lack of hysteresis.

One can apply the above theory to small particles when the particle size is so small that thermal energy $k_B T$ is much larger than KV. However if KV is larger or comparable to $k_B T$, it needs to be taken into account.

4.3 RELAXATION TIME

Consider an assembly of single domain particles. In the presence of an applied field, the particles approach an initial magnetization. Let the field is turned off at time t = 0.

The particles with thermal energy greater than anisotropy energy KV reverse their magnetization and net magnetization begins to decrease. The time rate of magnetization change will be directly proportional to the existing magnetization M at that time and to the Boltzmann factor $e^{-KV/kT}$. The Boltzmann factor is the probability of a particle that has enough energy to surmount the energy barrier $\Delta E = KV$ in order to reverse its magnetization.

$$-\frac{dM}{dt} = f_0 M e^{-KV/kT} \tag{4.1}$$

Negative sign shows that the magnetization decreases with the time. The proportionality constant f_0 is known as frequency factor and is about $10^9 sec^{-1}$. Equation 4.1 may be written as,

$$-\frac{dM}{dt} = \frac{M}{\tau}, \tag{4.2}$$

where τ is constant and is known as relaxation time.

$$\frac{1}{\tau} = f_0 e^{-KV/kT} \tag{4.3}$$

Integrate Equation 4.2 to get remanence M_r.

$$\int_{M_i}^{M_r} \frac{dM}{M} = -\int_0^t \frac{dt}{\tau} \tag{4.4}$$

$$\ln \frac{M_r}{M_i} = -\frac{t}{\tau},$$

$$M_r = M_i e^{-t/\tau} \tag{4.5}$$

Equation 4.5 shows that remanence magnetization M_r decreases to 1/e or 37% of its initial value during the relaxation time τ. Relaxation time τ is dependent on the volume of the particle and temperature from Equation 4.3.

4.4 BLOCKING TEMPERATURE (T_B)

Consider an example of spherical cobalt particles of diameter 68 A^0. The relaxation time at room temperature is calculated by substituting, $K = 45\times10^5$ ergs/cm^3, $V = 4\pi/3R^3 = 16.45\times10^{-20}cm^3$, $f_0 = 10^9 sec^{-1}$, and T = 300 K in Equation 4.3, we get $\tau = 10^{-1}$sec. Since the relaxation time is very small, the particles approach thermal equilibrium or zero magnetization in a very short time. Such behavior is the case for superparamagnetism that was discussed above in which KV is much smaller than k_BT. If the particle size increases to 90 A^0, the relaxation time jumps to 3.2×10^9 sec. Since τ is very large, the particles will remain stable for a longer time with fixed initial value of M_r. The above calculations show that a small change in particle size makes a large change in relaxation time.

To calculate the upper limit of volume V_p for superparamagnetic behavior, let the relaxation time of stable behavior be 100 sec. From Equation 4.3

$$10^{-2} = 10^9 e^{-\frac{KV_p}{kT}}$$

$$KV_p = 25kT \qquad (4.6)$$

For a particle such as cobalt the upper limit for superparamagnetism can be calculated from Equation 5, which will be 76 A^0 at room temperature.

Uniform size particles are characterized by a temperature T_B, called blocking temperature, below which particles are stable and ferromagnetic and above which are unstable and superparamagnetic. We consider $\tau = 100$ sec that yields

$$T_B = \frac{KV}{25k} \tag{4.7}$$

From the knowledge of upper limit particle size for superparamagnetism T_B can be calculated.

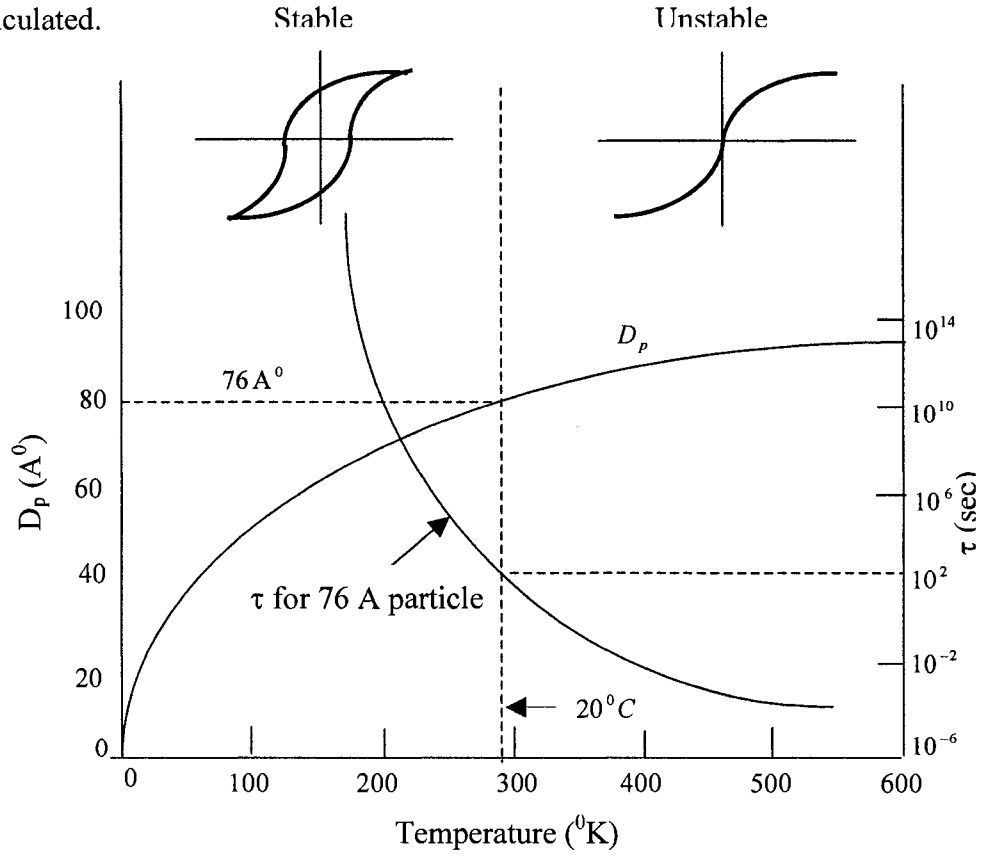

Figure 7. Temperature variation of the relaxation time and of critical diameter for spherical cobalt particles.

Figure 7 shows the critical diameter D_p of spherical cobalt particle versus temperature T and is explained by Equation 5 which state that cube of D_p is proportional to temperature. Similarly Figure 7 represents the relaxation time τ of cobalt particles versus temperature where τ varies exponentially with temperature and is given by Equation (4.3). The variation of critical diameter with temperature shows that 20^0 C is the blocking temperature for 7.6 nm particle diameter. At 20^0 C, the relaxation time is 100 sec. Below T_B and above 100 sec, the particles are stable. Above T_B and below 100 sec, the particles become unstable.

5.1 EFFECT OF AN APPLIED FIELD DURING EQUILIBRIUM

When the applied field compensates the thermal energy, particles reaches the saturation magnetization. Further increase in an applied field doesn't change the magnitude of magnetization. Consider an assembly of single domain particles initially saturated to easy axis along the +z direction. Let the reverse magnetization is carried along –z direction by an applied field. The magnetization vector of particles makes an angle θ with +z.

The total energy E of each particle is sum of anisotropy energy and potential energy.

$$E = V(K\sin^2\theta + HM_s\cos\theta) \tag{4.8}$$

To reverse the magnetization, particle has to surmount the energy barrier ΔE. The energy barrier is the difference between the maximum and minimum values of the total energy E.

$$\Delta E = E_{max} - E_{min} \tag{4.9}$$

Differentiating Equation 4.8 with respect to θ,

$$\frac{1}{V}\frac{dE}{dt} = 2K\sin\theta\cos\theta - HM_s\sin\theta = 0$$

$$\sin\theta\,(2K\cos\theta - HM_s) = 0$$

$$\sin\theta = 0 \text{ or } \cos\theta = \frac{HM_s}{2K}$$

The potential energy is minimum, when the particle is aligned parallel to easy axis. And $\theta = 0$. From Equation 4.8,

$$E_{min} = V\,H\,M_s \tag{4.10}$$

$\cos\theta = \frac{HM_s}{2K}$ is the condition for maximum energy where particles align antiparallel to easy axis. Substituting the value of $\cos\theta$ in Equation 4.8,

$$E_{max} = V\left(K + \frac{(HM_s)^2}{4K}\right) \tag{4.11}$$

Substituting Equation 4.10 and 4.11 in Equation 4.9

$$\Delta E = KV\left(1 - \frac{HM_s}{2K}\right)^2 \tag{4.12}$$

The energy barrier increases with the volume of particle and decreases with the applied field. Particle size greater than D_p does not reverse the magnetization but energy barrier can be reduced to 25kT with the applied field. This field will be the coercive field H_c given by

$$\Delta E = KV\left(1 - \frac{H_c M_s}{2K}\right)^2 = 25kT$$

$$H_c = \frac{2K}{M_s}\left[1 - \left(\frac{25kT}{KV}\right)^{1/2}\right] \tag{4.13}$$

When

$$T = \frac{KV}{25k};\ H_c = 0$$

As the particle size becomes very large or temperature approaches zero, coercive field becomes independent of an applied field and is reduced to $2K/M_s$. This coercive field is denoted by $H_{c,0}$.

$$H_{c,0} = \frac{2K}{M_s}$$

Reduced coercive field h_c is

$$h_c = \frac{H_c}{H_{c,0}} = 1 - \left(\frac{25kT}{KV}\right)^{1/2}$$

$$h_c = 1 - \left(\frac{V_p}{V}\right)^{1/2} = 1 - \left(\frac{D_p}{D}\right)^{3/2} \tag{4.14}$$

The coercive field increases as the particle diameter D increases beyond D_p.

Equation 4.14 gives the coercive field as a function of temperature and volume of the particles. Particle having critical size D_p or V_p have zero coercive field at their blocking temperature T_B and above.

In terms of temperature, the reduced coercive field is,

$$h_c = \frac{H_c}{H_{c,0}} = 1 - \left(\frac{25kT}{KV}\right)^{1/2}$$

Using Equation 4.7, the above equation becomes

$$h_c = 1 - \left(\frac{T}{T_B}\right)^{1/2} \tag{4.15}$$

The temperature dependence of the coercive field of single domain particles is shown in Figure 8.

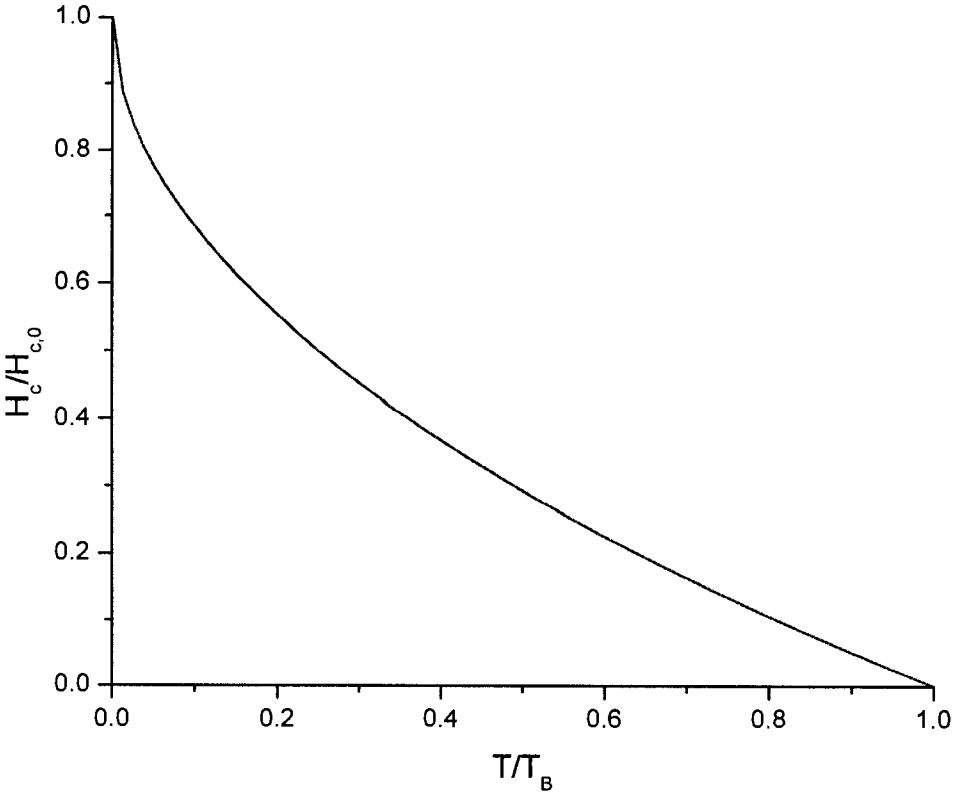

Figure 8. Temperature dependence of coercive field.

CHAPTER 5

NANOPARTICLES SYNTHESIS

5.1 SYNTHESIS OF MAGNETITE NANOPARTICLES (Fe_3O_4)

Dr. X.C. Sun from University of Alabama synthesized Fe_3O_4 nanoparticles that we used in present work. He also performed transmission electron microscopy and x-ray diffraction analysis. Below we describe briefly the synthesis method.

The synthesis procedure was based on the method developed by S. Sun and H. Zeng (2002). The main advantage of Sun and Zeng method is that the particles are nearly spherical in shape, equally distributed in size, and the desired size is easily controllable. The high temperature solution phase reaction takes place between 2 millimole of iron (III) acetylacetonate ($Fe(acac)_3$) and 20 mL of phenyl ether in presence of 10 mmol of 1,2-hexadecanediol, 6 mmol of oleic acid, and 6 mmol oleylamine. To avoid oxidation, the mixture is kept under the nitrogen environment. The refluxing is important to save the mixture from evaporating at high temperature; so at 260^0 C the mixture was refluxed for 30 minutes. A dark brown substance was produced when the solution was cooled down to room temperature, and treated with ethanol under air. The product was then dissolved in hexane, oleic acid, and oleylamine to remove unnecessary organic compounds. The subsequent introduction of ethanol to the product and its drying gave highly pure phase of 4 nm Fe_3O_4 nanocrystals in powder form.

CHAPTER 6

EXPERIMENTAL SYSTEMS

6.1 EQUIPMENTS

Our measurement system consists of a Lakeshore 4500 vibrating sample magnetometer, a Janice 153 cryogenic sample chamber, a lakeshore 340 temperature controller, BSL electromagnet, a tidewater magnet power supply, vacuum system, and a computer (Figure 11).

In VSM, the sample material is magnetized by a uniform horizontal magnetic field and the sample is made to undergo a periodic vertical motion with frequency of 60 Hz creating a time dependent magnetic field. The resulting time dependent magnetic flux induces a voltage in the nearby pick up coils, which is proportional to the magnetic moment of the sample. The voltage is processed by the VSM controller and sent to computer. A Hall probe is used to measure magnetic field, which operates based on Hall Effect.

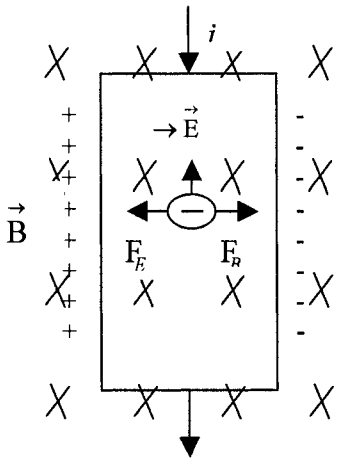

Figure 9. Hall effect.

When a current carrying conductor is placed in a magnetic field, the field will exert a magnetic force on moving electrons and pushes them to one side of the conductor by leaving the positive charge carriers on the other side. The separation of positive and negative charges gives rise to a voltage known as Hall voltage, which is proportional to applied field. The calculated voltage can be used for measuring magnetic field.

The electromagnet is connected to the bipolar power supply and water-cooling system. A current of 0 ± 49 Amp from power supply causes the magnetic field in the range 0 ± 10 kOe. A continuous water flow through the electromagnet keeps the magnet cool and protects the magnets from excessive heat.

We used a Janice 153 cryostat to cool the sample chamber from 4.2 – 300 K. The cryostat contains three concentric cylinders. The outer cylinder is used for generating a vacuum environment to insulate the interior from outside high temperature. The middle

cylinder holds the liquid helium, and the innermost cylinder is used for the sample.

Model 340 Lakeshore temperature controller is used to control the temperature of sample chamber from 4.2-300 K. The temperature controller supplies the power to the heater in the sample chamber. The temperature sensor (A Lakeshore TG-120-SD gallium-aluminum-arsenide (GaAlAs) diode) in the sample chamber located next to sample detects the temperature.

The vacuum and gas handling system consists of mechanical pumps, valves and vacuum lines. Such system is used to provide vacuum or transfer gas with appropriate pressure in the cryostat system chambers for specific reasons.

The VSM controller including the Hall probe and temperature controller are connected to computer using a National Instrument IEEE GPIB card. The combination of IEEE-GPIB software and a Lakeshore IDEAS VSM software two-way communication between the computer and various experimental systems is established. The following diagram shows the connection between the computer and VSM controller.

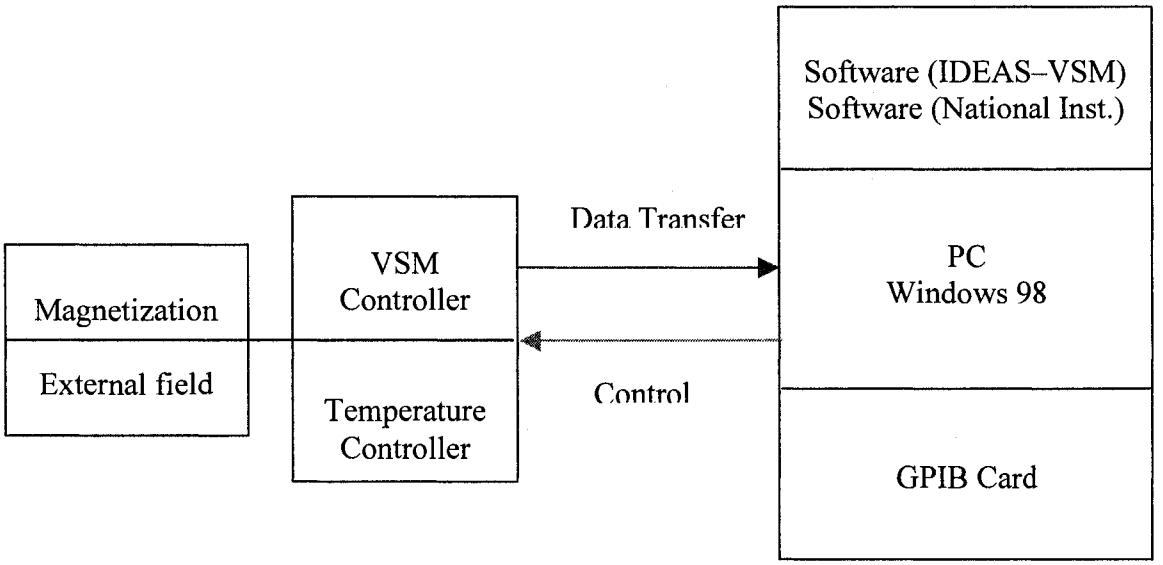

Figure 10. Block diagram of data acquisition.

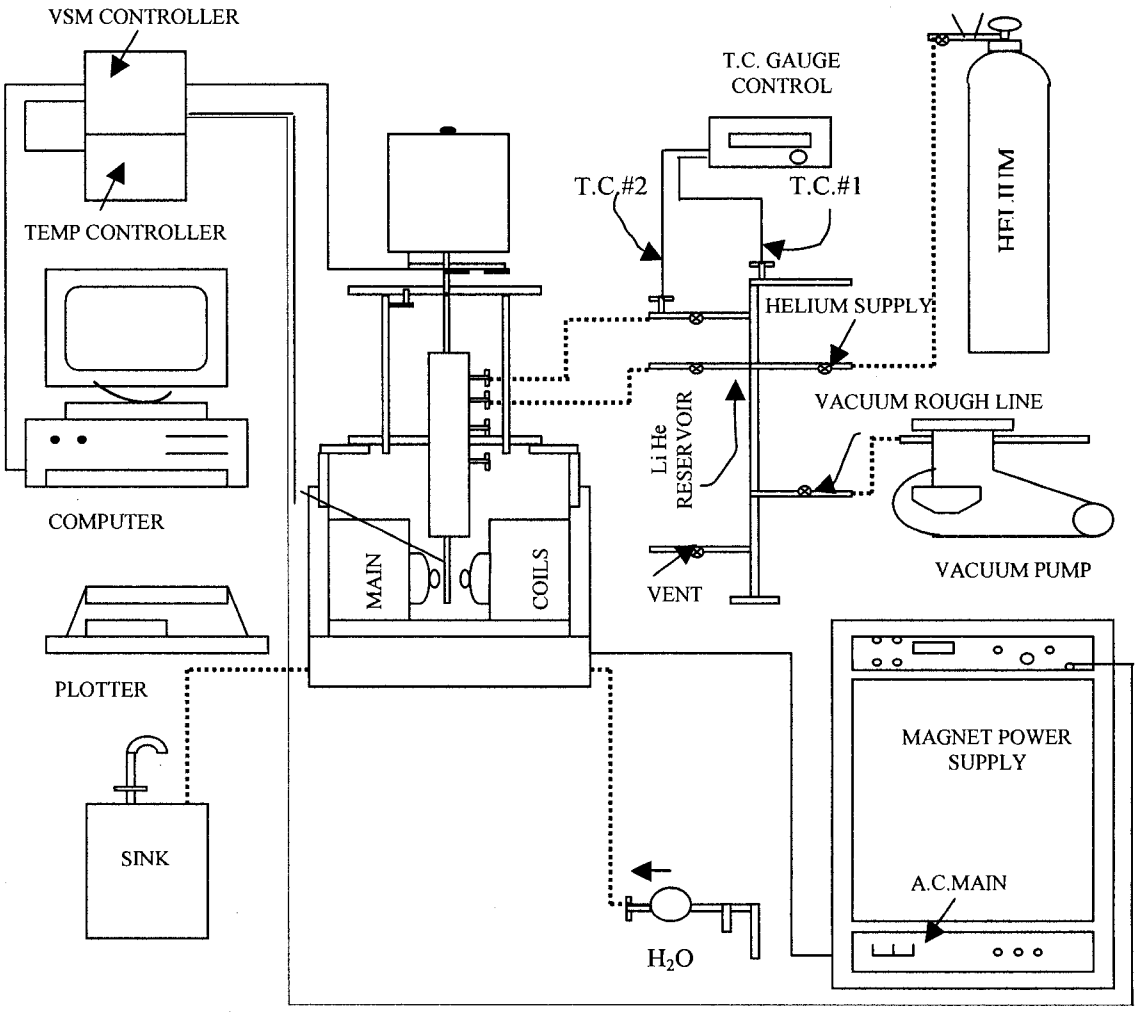

Figure 11. Low temperature VSM schematic

6.2 EXPERIMENTS

We used a VSM to measure the magnetic moment or magnetization of Fe_3O_4 nanoparticles. The measurements include the magnetization as a function of magnetic field in the range $0-\pm 10$ kOe at temperature in the range 4.2-160 K and magnetization

as a function of temperature also in the same temperature range at constant field of 100 Oe in zero-field-cooled and field-cooled conditions.

In a zero-field-cooled experiment (ZFC), first the sample is cooled to liquid helium temperature under zero external field. A small external field of 100 Oe is applied and net magnetization is measured as a function of temperature as the sample is heated from 4 K to 160 K. In the field-cooled (FC) experiment the sample is cooled in the presence of 100 Oe external field and magnetization versus temperature is measured as the temperature is cooled from 160 K to 4.2 K.

CHAPTER 7

EXPERIMENTS

7.1 X-RAY DIFFRACTION

Dr. X. C. Sun from University of Alabama performed x-ray diffraction (XRD) of Fe_3O_4 nanoparticles. The study was done on a Rigaku D/MAX-2BX horizontal XRD thin film diffractometer using Cu K_α as a target.

7.2 HIGH-ANGLE ANNULAR DARK-FIELD IMAGE

Dr. X. C. Sun from University of Alabama reports the high-angle annular dark-field (HAADF) images. The images were recorded using a JEOL 2010 STEM/TEM analytical electron microscope at 200 KV.

HAADF image is a type of image obtained from scanning transmission electron microscopy (STEM). It is a powerful technique for the investigation and identification of nanoscale materials. In STEM, a tiny, convergent electron beam is scanned over a defined area of the sample. HAADF detector detects electrons that are incoherently scattered to higher angles and contributes to image.

7.3 ENERGY DISPERSIVE SPECTROSCOPY

We performed the energy dispersive spectroscopy (EDS) using a FEI Quanta 200 scanning electron microscope to identify the elements and their percentage in a given sample (Postek, 1980). In this experiment the sample is exposed to a beam of electrons with the energy of about 20 keV, which knocks an electron with energy less than 20 keV from the inner shell of each atom. The hole created in the orbital is replaced by another electron from the high energy orbital. The energy difference between the high and low energy orbital emits in the form of electromagnetic radiation known as x-ray. The number of x-rays photons emitted from individual atoms are counted and plotted against the energy with peaks corresponding to each element present in the sample.

7.4 MAGNETIC MEASUREMENTS

First diluted low-temperature lakeshore varnish (VGE-7031) was gently poured into a 200 mil circular groove of a Kel-F sample holder. The powdered sample of magnetite nanoparticles synthesized by X.C. Sun was then poured into and mixed with the epoxy. As the epoxy dried out the particles were immobilized. The magnetization M as a function of temperature T was measured by varying the temperature from 4.2 K to 160 K in zero-field-cooled and from 160 K to 4.2 K in field cooled experiments at fixed field of 100 Oe. In another set of experiments the magnetization M as a function of field H was measured by varying the field from 0 to ± 10 KOe at fixed temperatures in the range from 6.5 K-100 K.

CHAPTER 8

RESULTS AND DISCUSSIONS

X-ray diffraction profile showed peaks compatible with those of Fe_3O_4 (Jade library from Materials Data, Inc. that gives Fe_3O_4 peaks) as shown in Figure 12. Using Scherrer formula (Klug and Alexander, 1962) we calculated the average particle size of 3.56 nm from width of the peaks. Scherrer equation gives the particle size of small crystals from the measured width of their diffraction curves. It is written as

$$t = \frac{K\lambda}{B\cos\theta_B}, \tag{8.1}$$

where t is the average dimension of particles, K is the Scherrer constant ($1 \geq K \geq 0.89$) and for calculation we consider $K = 1$, λ is the wavelength of x ray ($\lambda = 0.154$ nm), B is an angular width at an intensity equal to half the maximum intensity and θ_B is the Bragg angle (Cullity, 1978). Angular width and Bragg angle was measured for peak (220), (311), (400) and (422) as given by Figure 12. The size of the particle was calculated using Equation 8.1 and tabulated in Table 1. The calculated average size of the particle is 3.56 nm.

Table 1. Measured particle size using Scherrer formula

Peak	2θ	cosθ	B^0	t (nm)
220	30.5	0.965	2.75	2.99
311	35.0	0.954	2.50	3.33
400	43.5	0.929	2.00	4.28
422	57.5	0.877	2.25	3.66

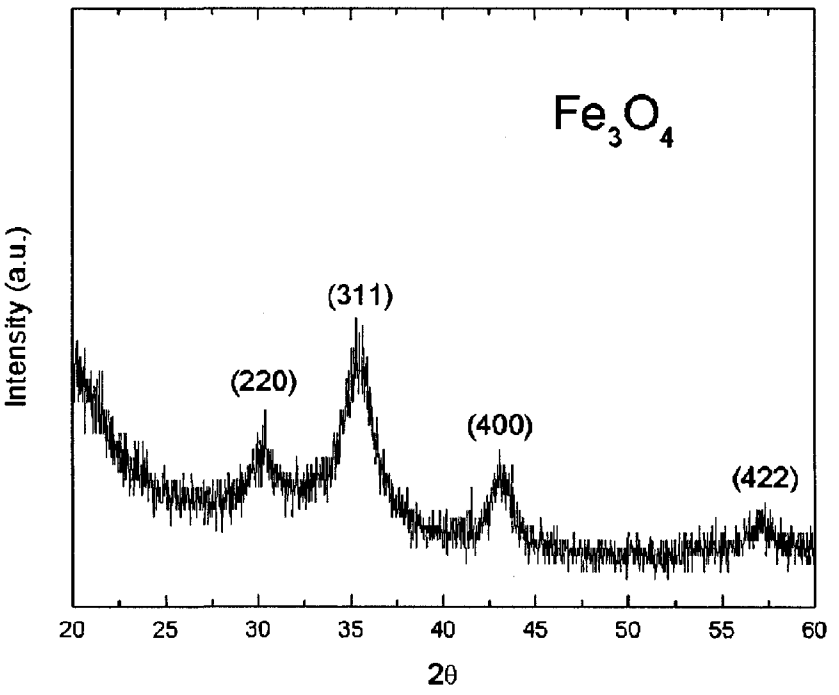

Figure 12. XRD pattern for as-prepared Fe_3O_4 particles (X.C. Sun).

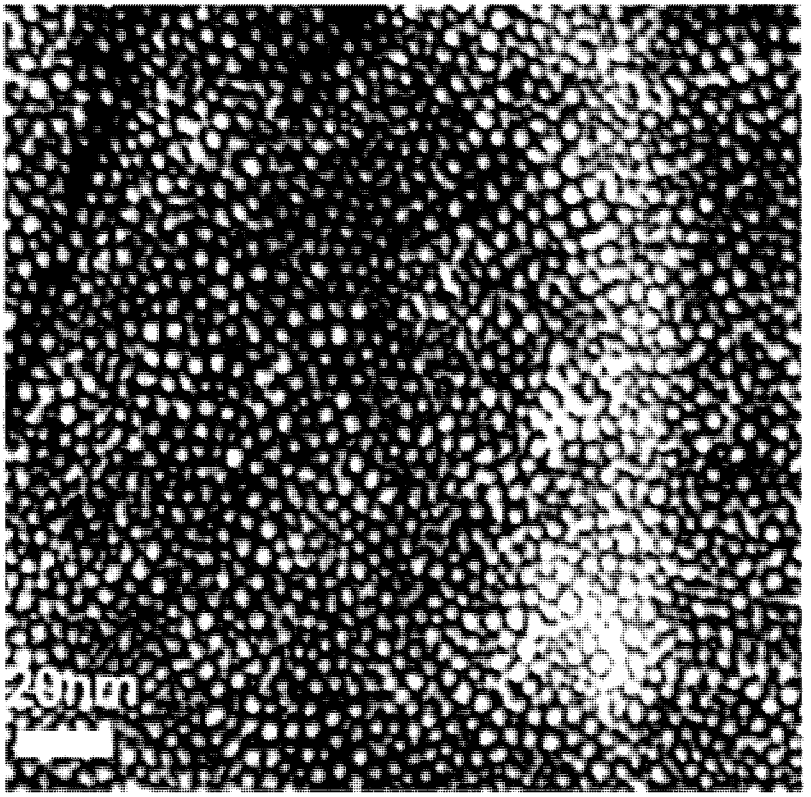

Figure 13. HAADF image of Fe_3O_4 particles (X.C. Sun).

The HAADF image (Figure 13) shows that the particles are of the same shape and size. The bar of 20 nm contains about eight particles, which gives 2.5 nm as the average size of each particle.

EDS spectrum of Fe_3O_4 (Figure 14) shows major peak of iron (Fe) and oxygen (O) that are due to K and L orbital. An addional peak is due to the Si substrate that we used for the sample. An atom of iron with Z = 26 has 2, 8, and 16 electrons in K, L, and M shells respectively. An x-ray, which is created by the filling of a vacancy in a K shell, is

termed as a K x-ray; the filling of an L shell creates an L x-ray. A K alpha (K_α) x-ray is produced from a transition of an electron from the L to the K shell and a K beta (K_β) x-ray is produced from a transition of an electron from the M to a K shell, etc (Goldstein, 2003). Therefore the gamma energies are larger than beta and alpha energies and it is written as $E_{K\gamma} > E_{K\beta} > E_{K\alpha}$.

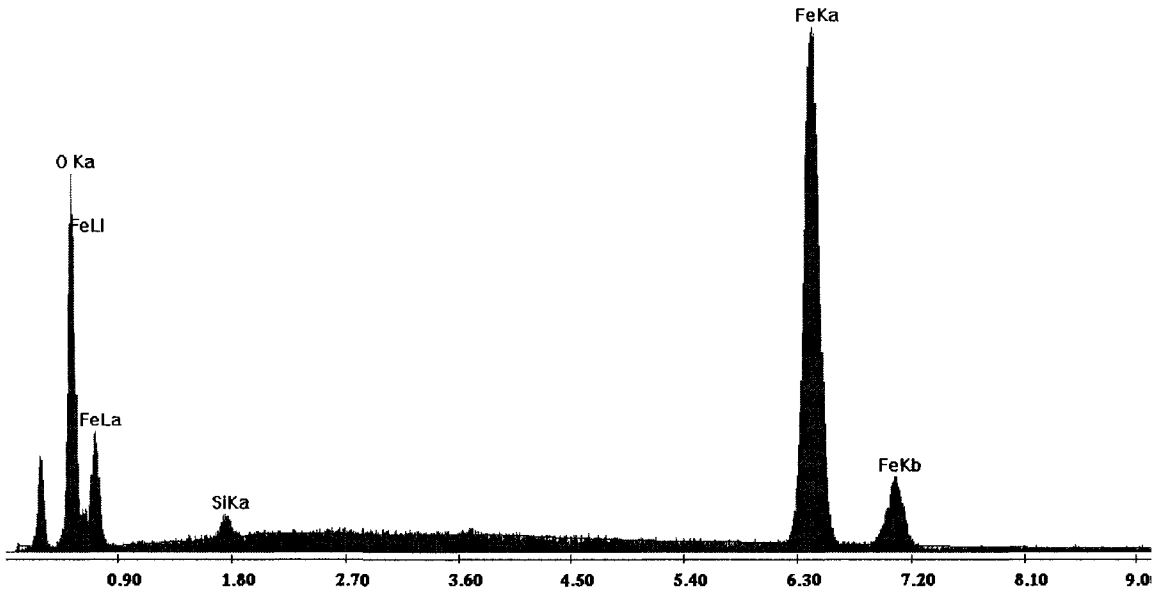

Figure 14. EDS spectrum of Fe_3O_4.

The experimental value of weight and atomic percentage of iron and oxygen is measured and compare with the expected result as in Table 2.

Table 2. Calculated and experimental weight & atomic percentage of Fe and O

	Calculated		Experimental	
Elements	Wt %	At %	Wt %	At %
Fe K	72.37	42.85	71.53	41.85
O K	27.62	57.14	28.47	58.85

The curves of M vs T in zero-field-cooled and field-cooled curve separate at 20 K indicating the blocking temperature of T_B = 20 K as shown in Figure 15.

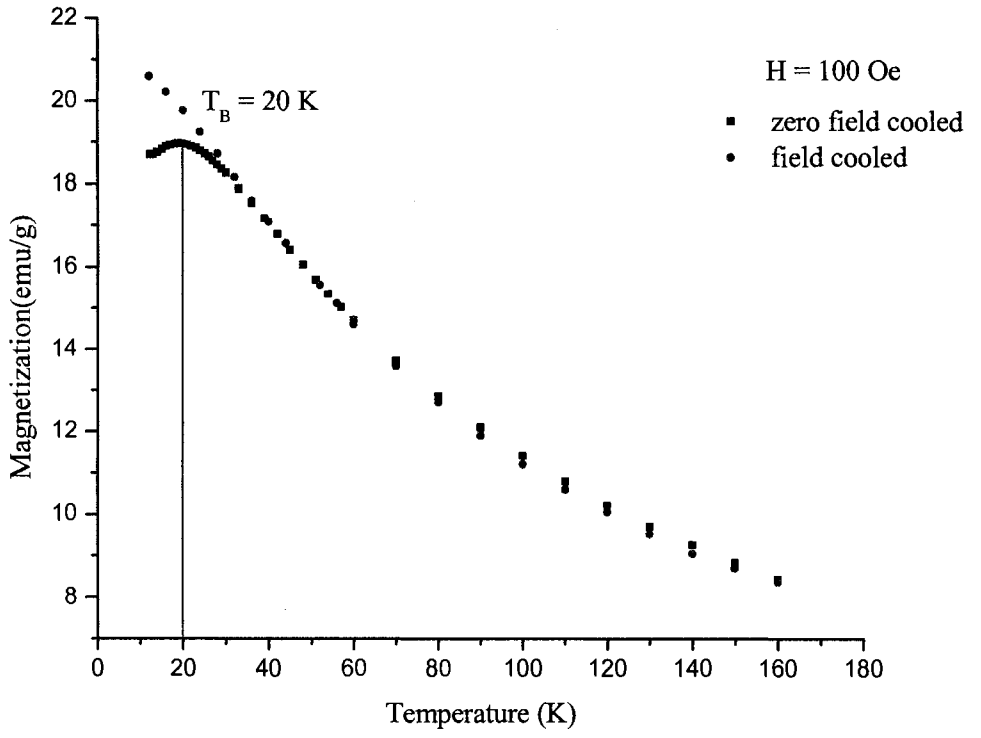

Figure 15. M vs T for field cooled (FC) and zero-field-cooled (ZFC) experiments.

The magnetization as a function of field was measured for temperatures 6.5-18.5 K below T_B in the steps of 4 K and for temperatures 25-100 K above T_B in the steps of 15 K. The open hysteresis loop below blocking temperature T_B shows that the particles are ferromagnetic with coercive field up to 400 Oe at 6.5 K (Figure 16). The coercive field drops to zero as temperature approaches blocking temperature T_B. The closed hysteresis loops above blocking temperature T_B reveal the superparamagnetism of particles. The overlapping M versus H/T curves for all M-H curves measured in the range 30-150 K above blocking temperature T_B are shown in Figure 17. The Langevin function $y = a(\coth(abx) - abx)$ with fitting parameter $M = y$, $M_0 = a$, $m/k_B = b$ is used for fitting gives the particle size of 4 nm and magnetization of 36.2 emu/g.

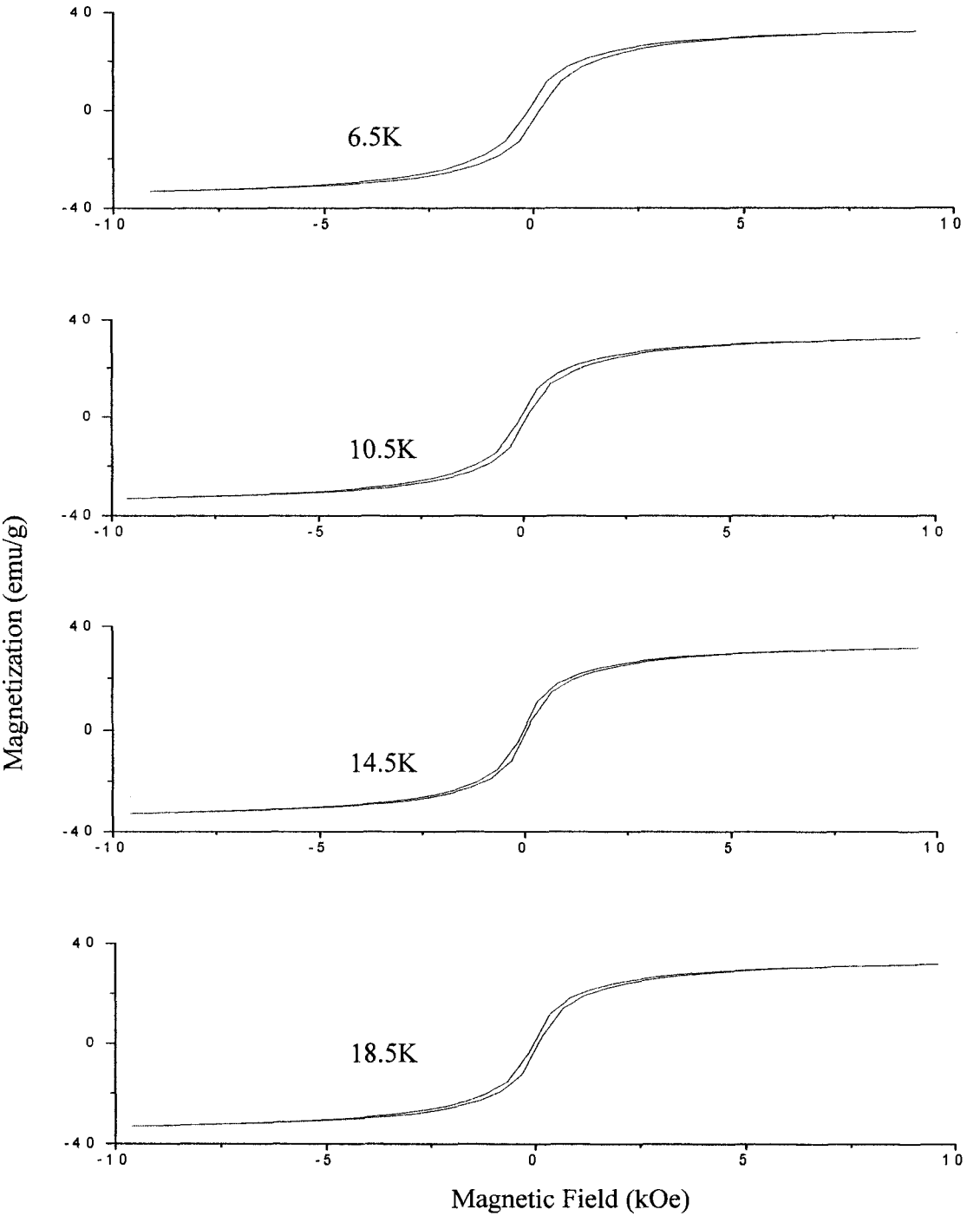

Figure 16. M vs H for temperature below blocking temperature showing the ferromagnetic behavior of the nanoparticles.

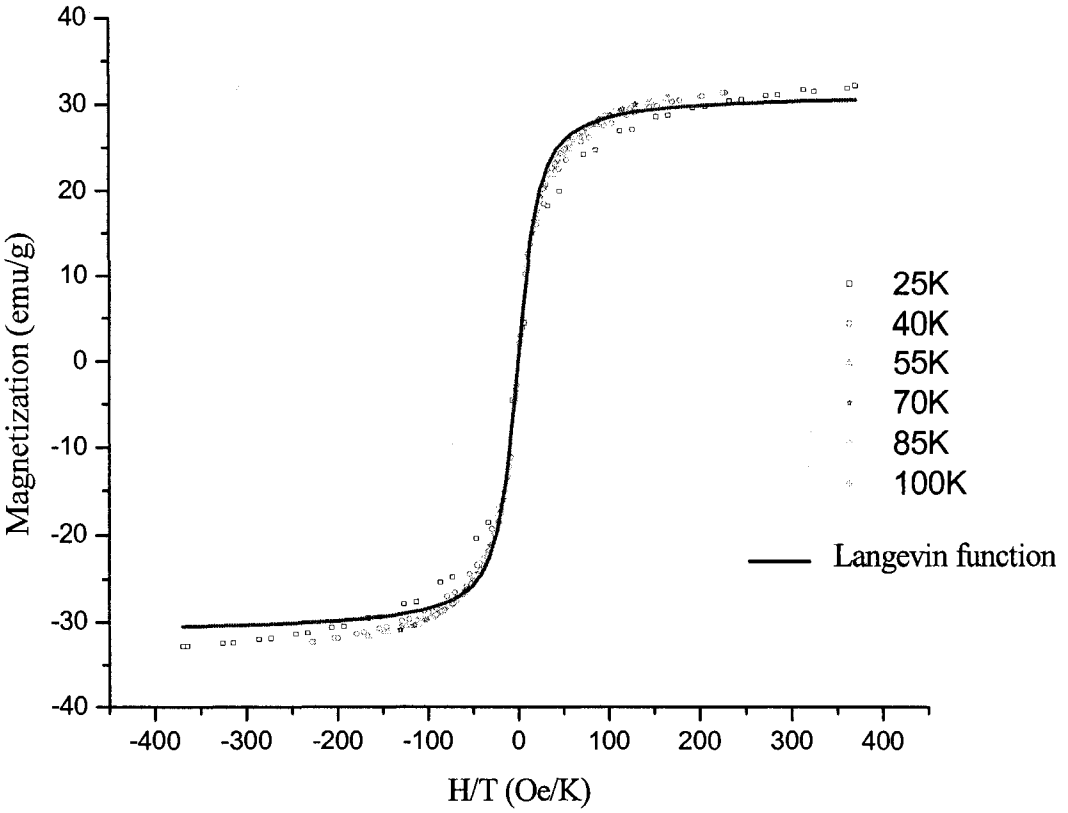

Figure 17. M vs H/T for temperature 25-100 K with the fitted Langevin function.

In order to observe the transition from ferromagnetism to superparamagnetism, zero-field- cooled (ZFC) and field-cooled (FC) experiments were performed on Fe_3O_4 nano-particles. Figure 15 shows that the sample is ferromagnetic below the blocking temperature $T_B = 20$ K and becomes superparamagnetic above T_B. The dependence of M versus T in ZFC experiment can be explained considering magnetocrystalline energy, Zeeman energy, and thermal energy where in various temperature ranges one is

significant.

When the sample is cooled to the lowest temperature in the absence of external field (ZFC), the moments align along the easy axis of crystal in the lattice. Since the grains or crystallites in the sample are oriented in random direction, the overall magnetic moment will be zero. If a small external field is applied at the lowest temperature, the magnetization is still remains at zero. As the temperature is increased, small fluctuation of moments due to thermal energy releases the moments from easy axis direction and moments start aligning along the external field. So at the lowest temperature magnetocrystalline energy (KV) is dominant. Further increase in temperature provides more thermal energy to moments and helps moments to overcome the magnetocrystalline energy. More and more moments orient along the direction of field. At specific temperature known as blocking temperature the largest number of moments are aligned with the external field and give maximum magnetization. Above this temperature the thermal energy $k_B T$ becomes stronger than the Zeeman energy and thermal vibration randomize the moments. As a result the net moment decreases with the increase in temperature beyond blocking temperature. In this temperature regime the particles are called superparamagnetic.

When the particles are cooled in the presence of small external field (FC), the decrease in thermal energy diminishes the thermal fluctuation of the moments. The moments start orienting along the direction of field and give rise to increase in magnetization. The field-cooled curve follows the zero-field curve as the temperature

decreases. At a specific temperature, the Zeeman energy overcomes the thermal energy and causes the moments to orient partially along the applied field. Due to this effect, instead of following zero-field cooled curve, field-cooled curve separate from it. The temperature where two curves separate is known as blocking temperature. Below T_B the thermal energy reduces as the temperature decreases and Zeeman energy become more effective. At the lowest temperature the Zeeman energy causes the maximum orientation of moments in the field direction.

We substitute $T_B = 20$ K and particle diameter of 3.56 nm from XRD result in Equation 4.7.

$$K = \frac{25kT_B}{V} \tag{8.2}$$

We obtain the anisotropy constant of $K = 29.2\times10^5$ erg/cm^3. The anisotropy constant of bulk Fe_3O_4 is 1.1×10^5 erg/cm^3 which is smaller than the calculated anisotropy constant of the nanoparticles. The difference is due to the surface anisotropy (Lin, Chiang, Wang, and Sung, 2006) of nanoparticles having a large surface to volume ratio.

M vs H measurements were done at temperature below the blocking temperature T_B. Figure 16 shows that the coercive field H_c decreases from maximum value of 190 Oe to zero at T_B. The coercive field is measured and plotted as a function of temperature (Figure 18).

From Equation 4.15

$$H_c = H_{c,0}\left(1 - \left(\frac{T}{T_B}\right)^{1/2}\right) \tag{8.3}$$

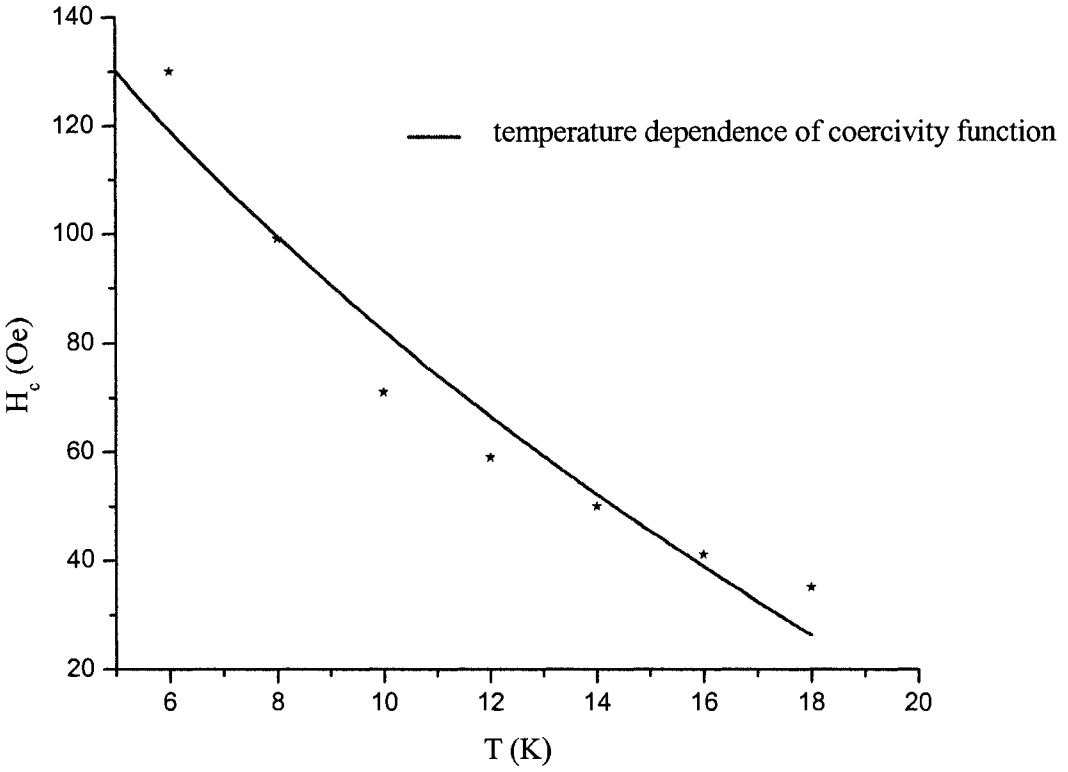

Figure 18. H_c vs T with fitted temperature dependence of coercivity function.

The data of coercive field versus temperature below T_B were fitted to the Equation 8.3 with T_B and $H_{c,0}$ as fitting parameters, and $T_B = 21$ K and $H_{c,0} = 344$ Oe were obtained.

M vs H measurements were done at constant temperatures above blocking temperature in the superparamagnetic regime. The magnetization is plotted as a function of H/T for all temperatures. Figure 17 shows that the all magnetization curves plotted against H/T superimpose on each other, which is the characteristic behavior of superparamagnetic particles. The corresponding data were fitted to Langevin function (Equation 3.8) with two fitting parameters $a = M_0$ and $b = \frac{m}{k_B}$.

We obtain $a = 33.352$ emu/g, $b = 0.00165$ g K/ergs. From value of b we calculated the mass of each particle $m = 2.277 \times 10^{-19}$ g. From the density of Fe_3O_4 sample $\rho = 5.046$ g/cm^3 the diameter of single particle is calculated as 4.41 nm. This result is consistent with the particle diameter 3.56 nm that was calculated from x-ray diffraction using Scherrer formula. The saturation magnetization of bulk Fe_3O_4 is 92 emu/g. The nanoparticle saturation magnetization obtained is 33.352 emu/g and is less than the bulk sample. As the particle size decreases, the surface to volume ratio increases and therefore surface effects dominants the magnetic properties of the smallest particles (Koseoly, Kavas, and Akta, 2006). In a particle of radius of 4 nm, 50% of atoms lie on the surface and therefore the surface effect become important. The magnetization near the surface is generally lower than in the interior (Berkowitz, Kodoma, Makhlouf, Parker, Spada, et al., 1999). In the core of the particle, the magnetization vector points along the easy axis of bulk material and gradually turns into

a different direction when it approaches the surface (Fiorani, 2005, Kachkachi, Ezzir, Nogues, and Tronc, 2000).

CHAPTER 9

SUMMARY

The structure and magnetic properties of Fe_3O_4 nanoparticles with average particle size of 3 nm synthesized by self-assembly method of Sun and Zeng were studied. The elemental analysis was done by energy dispersive spectroscopy (EDS) and the atomic percentiles of elements were consistent with the expected values. X-ray diffraction was done to verify the crystal structure and the peaks were compatible with those of Fe_3O_4. The width of the peaks gave the average size of nanoparticles as 3.56 nm using Scherrer formula. The transmission electron microscopy images showed that particles were almost spherical and the particle size distribution generated from the images gave the values close to that of XRD.

A vibrating sample magnetometer was used for measurement of magnetization versus field and temperature. Zero field cooled and field cooled measurements in the temperature range 4-160 K showed that the particles are superparamagnetic down to the blocking temperature of $T_B = 20$ K. At temperatures below T_B, nanoparticles are ferromagnetic as is evidenced by measured M-H hysteresis loops made in several temperatures in the range 6.5-18.5 K.

The coercive field of 400-160 Oe was also measured in this temperature range. For temperatures larger than blocking temperature M versus H/T curves at several temperatures were fitted to Langevin function for superparamagnetic nanoparticles. The fitting parameters gave the average size of particles as 4.41 nm and saturation magnetization of 33.352 emu/g, which is lower than that of bulk Fe_3O_4. The high surface to volume ratio of nanoparticles causes the saturation magnetization to be lower than that of bulk material. Also the anisotropy constant of magnetite was calculated from the size of particle obtained from x-ray diffraction result and blocking temperature T_B measured from ZFC and FC experiment and we obtained the value of 29.2×10^5 erg/cm^3, which is less than that of the bulk value. This difference comes from the surface effect of nanoparticles.

REFERENCES

Berkowitz, A. E., Kodoma, R. H., Makhlouf, S. A., Parker, F. T., Spada, F. E., E. J., et al. (1999). Anomalous Properties of Magnetic Nanoparticles. *J. Magn. Magn. Mater., 196*, 591.

Cullity, B. (1972). *Introduction to magnetic materials*. New York: Addison - Wesley.

Cullity, B. (1978). *Elements of x-rAy diffraction*. New York: Addison - Wesley.

Dravid, V., Host, J. J., Teng, M. H., Elliot, B. R., Hwang, J. H., Johnson, D. L., et al. (1995). Controlled-Size Nanocapsules. *Nature, 374*, 602.

Elkins,]. ., Li, D., Poudyal, N., Nandwana, V., Jin, Z., Chen, K., et al. (2005). Monodisperse Face-Centred Tetragonal FePt Nanoparticles with Giant Coercivity. *J. Phys. D: Appl. Phys., 38*, 2306 - 2309.

Fiorani, D. (Ed.). (2005). *Surface Effects in Magnetic Nanoparticles*. New York: Springer.

Gangopadhyay, S., Hadjipanayis, G. C., Dale, B., Sorensen, C. M., & , K. J.(1992). *Nanostruct. Mater., 1*, 77.

Goldstein, J. (2003). *Scanning Electron Microscopy and X-RayMmicroanalysis*. New York: Springer.

Gong, W., Li, H., Zhao, Z., & Chen, J. J.(1993). Ultrafine Particles of Fe, Co, and Ni Ferromagnetic Metals. *Journal of Applied Physics, 69*, 5119.

Hihara, T., Onodera, H., K.Sumiyama, K., K.Suzuki, K., Kasuya, A., Nishina, Y., et al. (1994). Magnetic Properties of Iron in Nanocapsules. *Jpn J. Appl. Phys., 33*, L24 - L25.

Jacobs, I., & Bean, C. (1963). Fine Particles, Thin Films and Exchange Anisotropy. *Magnetism, 111*, 271-350.

Kachkachi, H., Ezzir, A., Nogues, M., & Tronc, E.(2000). Surface Effects in Nanoparticles : Application to Maghemite γ-Fe_2O_3. *Eur. Phys. J., B14*, 681-689.

Kang, S., Harrell, J., & , D. N.(2002). Reduction of the FCC to L10 Ordering Temperature for Self-Asembled FePt Nanoparticles Containing Ag. *Nano. Lett. 2, 10*, 1033.

Klug, H., & , Alexander, L.(1962). *X-ray Diffraction Procedures for Polycrystalline and Amorphous Materials*. New York: Wiley.

Kneller, E., & Luborsky, F. (1963). Particle Size Dependence of Coercivity and Remanence of Single Domain Particles. *Journal of Applied Physics, 34*, 656-658.

Koseoly, Y., Kavas, H., & Akta, B.(2006). *Physica Status Solidi, Applied Research, 203*, 1595.

Lin, R. C., Chiang, R. K., Wang, J. S., & Sung, T. W.(2006). *J. Appl. Phys., 99*, 08N710.

Mchenry, M., Majetich, S., Artman, J., DeGraef, M., & Staley, S.(1994). Superparamagnetism in Carbon Coated Co Particles Produced by The Kratschmer Carbon Arc Process. *Physical Review, B49*, 11358-11363.

Neel, L.(1949). Influence des fluctuations thermiques sur l'aimantaion de grains ferromagnetiques tres fins. *Compt. Rend., 228*, 664-666.

Postek, M. (1980). *Scanning electron microscopy*. Ladd Research Industries.

Ruoff, R., Lorents, D., Chan, b., Malhotra, R., & Subramoney, S.(1993). Single Crystal Metals Encapsulated in Carbon Nanoparticles. *Science, 259*, 346.

Spaldin, N. (2003). *Magnetic materials*. United Kingdom: Cambridge University Press.

Subramoney, S., Ruoff, R., Lorents, D., Chan, B., Malhotra, R., Dyer, M., & Parvin, K.(1994). Single Crystal Metals Encapsulated in Carbon Nanoparticles . *Carbon 32*, 507.

Sun, S., Murray, C. (1999). Synthesis of Monodisperse Cobalt Nanocrystals and Their Assembly into Magnetic Superlattices. *Journal of Applied Physics, 85*, 4385.

Sun, S., Murray, . C., Weller, . D., Folks, . L., & , A. M.(2000). Monodisperse FePt Nanoparticles and Ferromagnetic FePt Nanoparticle Superlattice. *Science, 287*, 1989.

Sun, S., & Zeng, H.(2002). Size-Controlled Synthesis of Magnetite Nanoparticles. *J. Am. Chem. Soc., 124*, 8204.

Sun, S., Anders, S., Thomson, T., Baglin, J., Toney, M., Hamann, H., et al. (2003). Controlled Synthesis and Assembly of FePt Nanoparticles. *J. Phys. Chem.*, *107*, 5419.

Woods, S., Kirtley, J., Sun, S., & Koch, R.(2001). Direct Investigation of Superparamagnetism in Co Nanoparticle Films. *Physical Review Letters*, *87*, 137205.